Published in final edited form as:
IEEE Trans Med Imaging. 2007 April ; 26(4): 462–470. doi:10.1109/TMI.2005.853923.

Large Deformation Diffeomorphism and Momentum Based Hippocampal Shape Discrimination in Dementia of the Alzheimer type

Lei Wang[*],
Department of Psychiatry, Washington University School of Medicine, Campus Box 8134, 660 S. Euclid Ave, St. Louis, MO 63110 USA.

Faisal Beg,
School of Engineering Science, Simon Fraser University, Burnaby, BC V5A 1S6, Canada.

Tilak Ratnanather,
Institute for Computational Medicine, Center for Imaging Science, The Johns Hopkins University, Baltimore, MD 21218 USA.

Can Ceritoglu,
Center for Imaging Science, The Johns Hopkins University, Baltimore, MD 21218 USA.

Laurent Younes,
Institute for Computational Medicine, Center for Imaging Science, The Johns Hopkins University, Baltimore, MD 21218 USA.

John C. Morris,
Alzheimer Disease Research Center, Department of Neurology, Washington University School of Medicine, St. Louis, MO 63110 USA.

John G. Csernansky, and
Department of Psychiatry and Department of Anatomy & Neurobiology, Washington University School of Medicine, St. Louis, MO 63110 USA.

Michael I. Miller
Institute for Computational Medicine, Center for Imaging Science, The Johns Hopkins University, Baltimore, MD 21218 USA.

Abstract

In large-deformation diffeomorphic metric mapping (LDDMM), the diffeomorphic matching of images are modeled as evolution in time, or a flow, of an associated smooth velocity vector field v controlling the evolution. The initial momentum parameterizes the whole geodesic and encodes the shape and form of the target image. Thus, methods such as principal component analysis (PCA) of the initial momentum leads to analysis of anatomical shape and form in target images without being restricted to small-deformation assumption in the analysis of linear displacements. We apply this approach to a study of dementia of the Alzheimer type (DAT). The left hippocampus in the DAT group shows significant shape abnormality while the right hippocampus shows similar pattern of abnormality. Further, PCA of the initial momentum leads to correct classification of 12 out of 18 DAT subjects and 22 out of 26 control subjects.

[*] lei@wustl.edu .

Keywords

Alzheimer's disease; geodesic; LDDMM; momentum; PCA

I. Introduction

AN important task in the field of computational anatomy (CA) [1] is the study of neuroanatomical variability. In CA, the anatomic model is a quadruple $(\Omega, \mathcal{G}, \mathcal{I}, \mathcal{P})$ consisting of $\Omega \subset \mathbb{R}^3$ the template coordinate space, defined as the union of 0-D, 1-D, 2-D, and 3-D manifolds, $\mathcal{G}:\Omega \leftrightarrow \Omega$ a set diffeomorphic transformations on Ω, $\mathcal{I}$ the space of anatomies, is the orbit of a template anatomy I_0 under $\mathcal{G}$, and $\mathcal{P}$ the family of probability measures on $\mathcal{G}$. In this framework, a geodesic $\phi: [0, 1] \rightarrow \mathcal{G}$ is computed where each point $\phi_t \in \mathcal{G}$, $t \in [0,1]$ is a diffeomorphism of the domain Ω. The evolution of the template image I_0 along the path is given by $\phi_t I_0 = I_0 \circ \phi_t^{-1}$ such that the end point of the geodesic connects the template I_0 to the target I_1 via $I_1 = \phi_1 I_0 = I_0 \circ \phi_1^{-1}$. Thus, anatomical variability in the target is encoded by these geodesic transformations when a template is fixed. Fig. 1 illustrates a schematic of the large deformation trajectory $\boldsymbol{\phi}_t(x)$ followed by a particle $x \in \Omega$ and its associated velocity vector field $v_t(\boldsymbol{\phi}_t(x))$.

Until now, we have been using displacement vector fields, $u:\Omega \rightarrow \mathbb{R}^3$ between the target and the template obtained from the matching transformation via $u = \boldsymbol{\phi}_1 - \boldsymbol{\phi}_0 = \boldsymbol{\phi}_1 - id$, where id is the identity transformation on Ω such that $id(x) = x$. These differences have been used to make statistical inferences (for work on Alzheimer's disease (AD), see [2]-[7]). While the transformations that we have been computing follow the large deformation approach in that they are the result of the evolution of a smooth time-dependent velocity vector field, the final shape analysis via linearizing around template coordinates using displacement vector fields has provided a practical basis for this approach [1].

Recent work in understanding diffeomorphic flows [8]-[10] has provided computational tools for comparing these geodesic transformations and deriving a fundamental "conservation of momentum" property of these geodesics. This property applies the general theory on invariant Riemannian metrics on transformation groups [11], and provides the theoretical background for parameterizing the entire geodesic by the initial momentum with which the optimal trajectory emanates from the template image coordinates to reach the target image. Anatomical submanifolds can now be compared by performing linear statistics on these initial momentum. This was illustrated by diffeomorphic mapping of surface submanifolds of the human heart [12] in volume space and face [13] in point space (sparse 1-D landmark sets) rather than volume.

In both [12] and [13], intrinsic average anatomies were constructed from the population under study and the population variation was studied as characterized by linear statistics. In this paper, we present diffeomorphic mappings of 3-D volumetric manifolds (hippocampus) and the linear statistics with discrimination on the initial momentum in the context of dementia of the Alzheimer type (DAT).

II. Methods

A. Large-Deformation Diffeomorphic Metric Mapping (LDDMM)

We have been estimating diffeomorphisms for template matching via the basic variational problem that, in the space of smooth velocity vector fields V on domain $\Omega \subset \mathbb{R}^3$, takes the form [9]

$$\widehat{v}=\underset{v:\dot{\phi}_t=v_t(\phi_t)}{\operatorname{argmin}}\left(\int_0^1\|v_t\|_V^2dt+\underbrace{\frac{1}{\sigma^2}\|I_0\circ\phi_1^{-1}-I_1\|_{L^2}^2}_{E_2}\right). \tag{1}$$

The optimizer of this cost then generates the optimal change of coordinates $\varphi=\widehat{\phi_1^v}$ upon integration $d\widehat{\phi_t^v}/dt=\widehat{v_t}\left(\widehat{\phi_t^v}\right)$, $\phi_0 = id$, where the superscript v in ϕ^v is used to explicitly denote the dependence of ϕ on the associated velocity field v. Enforcing a sufficient amount of smoothness on the elements of V ensures that the solution to the differential equation $\dot{\phi}=v_t(\phi_t)$, $t\in[0,1]$, $v_t\in V$ is in the space of diffeomorphisms [14,15]. The required smoothness is enforced by defining the norm on V through a 3×3 differential operator L of the type $L=(-\alpha\Delta+\gamma)^\alpha I_{3\times 3}$ where $\alpha > 1.5$ in 3-D space such that $\|f\|_V=\|Lf\|_{L_2}$, and $\|\cdot\|_{L_2}$ is the standard L_2 norm for square integrable functions defined on Ω. The differential operator L has periodic boundary conditions on a rectangular domain Ω. The gradient of this cost, in V, is given by

$$\nabla_v E_t=2\widehat{v_t}-K\left(\frac{2}{\sigma^2}|D\widehat{\phi_{t,1}^v}|\nabla J_t^0\left(J_t^0-J_t^1\right)\right) \tag{2}$$

where $J_t^0=I_0\circ\phi_{t,0}$ and $J_t^1=I_1\circ\phi_{t,1}$, $|Dg|$ is the determinant of the Jacobian matrix and K is a compact self-adjoint operator $K:L_2\left(\Omega,\mathbb{R}^3\right)\to V$ uniquely defined by $\langle a,b\rangle_{L_2}=\langle Ka,b\rangle_V$ such that for any smooth vector field $f\in V$, $K(L^\dagger L)f=f$ holds. The notation $\phi_{s,t}=\phi_s\cdot\phi_t^{-1}$ is also used. The $1/\sigma^2$ parameter in (1) provides weighted optimization between the regularization and the data matching components, and is chosen to be the same for all matchings.

B. Comparison Between LDDMM and Christensen's Greedy Algorithm

Large deformation flows first put forth by Christensen et.al. [16] generate paths through the space of diffeomorphisms matching the corresponding images. This algorithm exploits the fact that if the operator L is not differentiable in time, then the space-time $\Omega\times T$ is discretized into a sequence of time-indexed optimizations. The algorithm then solves for the locally optimal velocity at each time point and then forward integrates the solution. This is only a locally-in-time optimal method (therefore, the term "greedy") reducing the dimension of the optimization. The transformation $\phi_{1,0}$ matching the images is generated from velocity fields whose computation can be interpreted as following the variational Riemannian gradient of the data term E_2 in (1) [17]

$$\frac{\partial\phi_t}{\partial t}=v_t\circ\phi_t=-\nabla E_2(\phi_t). \tag{3}$$

This Riemannian (sometimes called "natural") gradient $\nabla E_2(\phi t)$ in the space of diffeomorphisms is given by

$$v_t=-\nabla E_2(\phi_t)\circ\phi_t^{-1}=\frac{2}{\sigma^2}K\left(\left(J_t^0-J_1^1\right)\nabla J_t^0\right) \tag{4}$$

where $J_t^0=I_0\circ\phi_{t,0}$ and $J_1^1=I_1$. The time-indexed sequence of locally optimal velocity fields v_{t_j} are integrated to yield the sequence of transformations $\phi_{t_j}^v$, $j=0,1,2,\ldots$, which are points along a path on the manifold of diffeomorphisms from the identity transformation to $\phi_{1,0}$

matching the given images. The regularization provided by the smoothing operator K gives this gradient numerically stable behavior in finite time.

The main difference between the greedy and the LDDMM algorithms is that the path generated by the greedy method does not correspond to any global variational problem solution given by (1). As a result, the greedy method in general will not generate the shortest path connecting the images through the space of diffeomorphisms. Further, unlike LDDMM, the greedy method cannot generate metric distances between objects in the orbit [9], [18]. Metric distances between objects generated by LDDMM will be the focus of another paper. For in-depth comparison of these two algorithms, refer to [9].

C. Initial Momentum: Geodesic 3-D Evolution

The LDDMM algorithm, which is based on following a gradient in space of time-dependent smooth velocity fields, has yet another important distinction with respect to the greedy algorithm. The LDDMM geodesic follows the property of conservation of momentum [10] that is not shared by the locally optimal paths generated by the greedy algorithm. This property takes the form

$$\left(L^{\dagger}L\right)v_t=|D\phi_{t,0}|(D\phi_{t,0})^t\left(L^{\dagger}L\right)v_0\circ\phi_{t,0} \tag{5}$$

where $(L^{\dagger}L)\,v_t$ denotes the momentum of the evolving template transformation at time t. The knowledge of the initial momentum $(L^{\dagger}L)\,v_0$ with which the template coordinates evolve at $t = 0$ completely specifies the full geodesic connecting the given template and target imagery [10]. Hence, the initial momentum encodes the shape and form of the target. As also shown earlier [13] in the context of diffeomorphic evolutions of landmarks, linear combinations of momenta when propagated through the diffeomorphic evolution equations guarantee that the computed transformations will be diffeomorphic. The linearizing model encodes transformations via displacement fields in the coordinates of the fixed template. Transformations encoded this way are not guaranteed to remain diffeomorphic, at hence, the transformed template is not guaranteed to remain in the anatomical shape space as fusions, fold-overs and tears of anatomical structures can occur in this setting. In contrast, the LDDMM geodesic following the conservation of momentum whereby the matching transformations are completely encoded by the initial momentum in the template coordinates gives a powerful tool for studying shape variation, overcoming the restrictive assumption of linear displacement model and giving due consideration to the nonlinearity of the anatomical shape space. In particular, this allows linear techniques such as principal component analysis (PCA) to be applied to statistical analysis of the initial momentum that encodes the target shape.

D. PCA on the Initial Momentum

Hitherto we have used the linear displacement vector fields to compute PCA for the analysis of hippocampal shape [4], [7], [19]. However, displacement vector fields do not necessarily lead to diffeomorphic transformations, therefore, the assumption of small deformation had to be made [1]. To date, this assumption has not been severely tested since all of our study cases involved difference or changes in the hippocampus were not very large.

However, when the small-deformation assumption is removed, linear combination of the principal components $\widehat{u}^i=\sum_{k=1}^{N}\alpha_k^i e_k$ may breakdown when cross-subject differences are large [13]. That is, under mapping $\widehat{u}^i$ structures may not be able to relate to the template via a diffeomorphism.

We now extend the construction of orthonormal basis functions (i.e., PCA) of linear displacements on surface manifolds by Joshi [19] to PCA of initial momentum [see (5)] on volume manifolds [12]. Instead of performing PCA analysis under the L^2 metric, we perform it with respect to the metric in space V used for the estimation of the flow, i.e., $\langle v,w\rangle_V = \langle L^\dagger Lv,w\rangle_{L_2} = \langle Lv,Lw\rangle_{L_2}$, $v, w \in V$, the Hilbert space of smooth velocity vector fields. Thus, PCA is applied on the quantity Lv_0

Let $\mathcal{M}_0$ be the template volume manifold in $\Omega \subset \mathbb{R}^3$ (e.g., 3-D volumetric representation of the hippocampus). It follows that if $Y(x) = \{Lv^1(x), \ldots, Lv^N(x)\}$, $x \in \mathcal{M}_0$, is assumed to be a family of zero-mean1 Gaussian random vector fields on the manifold $\mathcal{M}_0$ with a covariance structure $K_Y(x,y)$, $x, y \in \mathcal{M}_0$ then the integral equation

$$\lambda_k e_k(x) = \int_{\mathcal{M}_0} K_Y(x,y)\, e_k(y)\, dy, \quad k=1,\ldots,N \tag{6}$$

has a solution of a set of orthonormal functions $\{e_1(x), \ldots, e_N(x)\}$, $x \in \mathcal{M}_0$ that is the minimizer of the following minimum mean-square error problem:

$$\underset{\{e_k\}}{\operatorname{argmin}}\, E\left\{\int_{\mathcal{M}_0}\left\|Y(x) - \sum_{k=1}^{N} A_k e_k(x)\right\|^2 dx\right\} \tag{7}$$

where

$$\begin{aligned} A_k &= \left\{\alpha_k^1,\ldots,\alpha_k^N\right\} \\ &= \int_{\mathcal{M}_0} (e_k(x))^T Y(x)\, dx \\ k &= 1,\ldots,N \end{aligned} \tag{8}$$

and dx is the measure on the manifold $\mathcal{M}_0$. The proof [20] follows the standard Karhunen-Loéve expansion [21]. This is the PCA, where $Y(x)$ is projected onto a subspace spanned by the orthonormal basis functions $\{e_1(x), \ldots, e_N(x)\}$, such that the residual error between $V(x)$ and the projection $\sum_{k=1}^{N} A_k e_k(x)$ is minimized [see (7)]. The set of scalars $\{A_k\}$, $k = 1, \ldots, N$, are the principal component values.

In discrete image space, the integral (6) becomes, at each voxel x

$$\lambda_k e_k(x) = \sum_l \widehat{K}_Y(x,y_l)\, e_k(y_l)\, dy_l, \quad k=1,\ldots,N \tag{9}$$

where dy_l is the measure around voxel y_l (i.e., voxel size) and $\widehat{K}_Y(x,y) = (1/N-1)\sum_{i=1}^{N} Lv^i(x)\, Lv^i(y)^T$ is the sample covariance.

The orthonormal basis $\{e_1(x), \ldots, e_N(x)\}$ is computed via the singular value decomposition (SVD) of Y as follows [19]. Let Y be the matrix of the vector fields with the mean subtracted, containing p rows and N columns ($p = 3 \times$ number of 3 -D image points, $N =$ number of subjects, $p > N$; for an image space of $64 \times 112 \times 64$ voxels, $p \approx 0.5 \times 10^6$), then the SVD of Y is defined as $Y = PDQ^T$, where $P^TP = I$, $Q^TQ = I$ and D is a diagonal matrix consisting of the singular values of Y. The singular values are related to the eigen-decomposition of $\widehat{K}$ as follows. We re-write the sample covariance as $\widehat{K} = (1/N-1)\, YY^T$. From the SVD equation of $Y = PDQ^T$ we see that $YY^T = PD^2P^T$. Thus, the eigenvectors of

[1] In practice we subtract the mean from the vector fields first.

$\widehat{K}$ are the column vectors of P up to a constant scaling factor, and the eigenvalues of the square matrix $\widehat{K}$ are the squares of the singular values of Y, up to a constant scaling factor. The matrix Q represents a directional component which is essentially ignored in the eigen-decomposition of $\widehat{K}$.

The first M, $M < N$, principal components (whose values are $\alpha_k^i = \sum_l (e_k(y_l))^T L v^i(y_l)\, dy_l$, $k = 1, \ldots, M$, $i = 1, \ldots, N$) that account for majority of the total variance (e.g., ~80%) are used in a nonparametric permutation test to determine if the shape of the hippocampus as represented by these principal components are statistically different between the subject groups.

E. Nonparametric Statistical Test

Let $\bar{\tilde{Z}}^{\text{Ctrl}} = \left\{ \bar{\alpha}_1^i, \ldots, \bar{\alpha}_M^i \right\}_{i=1,\ldots,N_{\text{Ctrl}}}$ and $\bar{\tilde{Z}}^{\text{DAT}} = \left\{ \bar{\alpha}_1^j, \ldots, \bar{\alpha}_M^j \right\}_{j=1,\ldots,N_{\text{DAT}}}$ be the sample means of the first M principal component values for each group, and $\widehat{\Sigma}$ the pooled (common) sample covariance. To test the null hypothesis

$$\mathcal{H}_0 : \bar{Z}^{\text{Ctrl}} = \bar{Z}^{\text{DAT}}$$

we compute the Hötelling's T^2 statistic [22] (for two samples) as

$$T^2 \doteq \frac{N_{\text{Ctrl}} N_{\text{DAT}}}{N_{\text{Ctrl}} + N_{\text{DAT}}} \times \left(\bar{\tilde{Z}}^{\text{DAT}} - \bar{\tilde{Z}}^{\text{Ctrl}} \right)^T \widehat{\Sigma}^{-1} \left(\bar{\tilde{Z}}^{\text{Ctrl}} - \bar{\tilde{Z}}^{\text{DAT}} \right). \tag{10}$$

The significance of group variation is measured in a permutation test as follows.

In Fisher's method of randomization, for all permutations of the given two groups, new means and covariances are calculated. Monte Carlo simulations are used to generate a large number of uniformly distributed random permutations (a typical number is 10 000). The collection of T^2 statistics from each permutation gives rise to an empirical distribution $\widehat{F}(\cdot)$ according to

$$F_{M, N_{\text{Ctrl}} + N_{\text{DAT}} - M - 1} = \frac{N_{\text{Ctrl}} + N_{\text{DAT}} - M - 1}{(N_{\text{Ctrl}} + N_{\text{DAT}} - 2) M} T^2. \tag{11}$$

The null hypothesis that the two groups have equal distributions is rejected when

$$p = \int_{T^2}^{\infty} \widehat{F}(f)\, df \tag{12}$$

falls below a predefined significance level (e.g., 0.05).

F. Subjects and Scans

The neuroanatomical template is produced using an MR image from an elder control subject. The subject selected to produce this template is obtained from the same source as the other subjects in the study, but is not otherwise included in the data analysis. The left and right hippocampi in this template scan have been manually segmented by a team of experts using methods previously described [23]. A more detailed anatomical description of the hippocampus as outlined in MR was also given in App. A of [24].

The initial hippocampal data used in this study came from our previously published longitudinal study of hippocampal atrophy in early DAT [4], where 18 very mild DAT (Clinical Dementia Rating Scale [25], CDR 0.5) subjects and 26 age-matched nondemented (CDR 0) controls had two MR scans approximately two years apart. To obtain the rating, an experienced clinician conducted semi-structured interviews with an informant and the subject to assess the subject's cognitive and functional performance; a neurological examination also was obtained. The clinician determined the presence or absence of dementia and, when present, its severity with the Clinical Dementia Rating (CDR), where CDR 0 indicated no dementia and CDR 0.5, 1, 2, and 3 indicated very mild, mild, moderate, and severe dementia [25]. The clinical diagnosis of DAT was in accordance with standard criteria and was verified by the neuropathologic diagnosis of AD in 93% of cases [26]. Although elsewhere the CDR 0.5 individuals in our sample may be considered to have mild cognitive impairment [27], they fulfill our diagnostic criteria for very mild DAT and at autopsy overwhelmingly have neuropathologic AD [28].

The mean [standard deviation (SD)] age for the CDR 0 group was 73 (7.0) years, and for the CDR 0.5 group, 74 (4.4) years. The gender distribution (M/F) of the subjects was CDR 0: 12/14, CDR 0.5: 11/7. The mean (SD) sum-of-boxes scores for the CDR 0 group was 0.02 (0.10), and for the CDR 0.5 group, 2.0 (1.3). All subjects had MR scans approximately two years apart—the mean scan interval for the CDR 0 group was 2.2 years (range 1.4–4.1 years), and for the CDR 0.5 group, 2.0 years (range 1.0–2.6 years). The scans were obtained using a Magnetom SP-4000 1.5 Tesla imaging system, a standard head coil, and a magnetization prepared rapid gradient echo (MPRAGE) sequence. The MPRAGE sequence (TR/TE—10/4, ACQ—1, Matrix—256 × 256, 180 slices, Scanning time—11.0 min) produced 3-D data with a 1 mm × 1 mm in-plane resolution and 1 mm slice thickness across the entire cranium.

In that study, baseline hippocampal surfaces were generated based on Christensen's greedy algorithm implementation of the diffeomorphic mapping from the above template. A comparison between the two groups at baseline is illustrated in Fig. 4 (1a) and (1b). The comparison is based on the surface displacement between each subject and the template, and computing the z-scores between the two subject groups. It has been shown that this pattern can be explained in terms of known AD pathology [4], [7].

In this study, we apply LDDMM to each template-target subject pair, taken from [4] at baseline to generate geodesics. To do so, the individual hippocampal surfaces already generated in each subject's scan are scaled by a factor of 2 and aligned with the template surfaces, similarly scaled, via a rigid-body rotation and translation. These surfaces are then converted into voxelized binary segmentations of dimension 64 × 112 × 64 which have isotropic voxel resolutions of 0.5 × 0.5 × 0.5 mm^3/ After smoothing by a Gaussian filter (9 × 9 × 9-voxel window and 1-voxel standard deviation), the voxelized binary segmentations have real intensity values ranging from 0 to 255. Then LDDMM is applied to each template-subject pair. Geodesics and initial momenta are generated as a result for each subject in the template coordinate space. PCA is then performed on these initial momenta after the mean has been subtracted.

III. Results

A. Validation 1: LDDMM Versus Greedy Algorithm

We have previously validated the accuracy of the automatic segmentations of the greedy algorithm by comparing with reference segmentations generated by trained individuals [23]. For measuring the accuracy, we define an L_1 error between positive summable functions [29], [30] (i.e., segmentations) as follows. Let $\mathscr{R}$ and $\mathscr{A}$ be reference manual and automated

segmentations of the image, respectively, such that each of the m-compartments is labeled with a tag ranging from 1 to m. For example, let $m = 3$, then 1 = *CSF*, 2 = gray matter, 3 = white matter. Let $p^{\mathcal{R}}(h_n|I_n)$ and $p^{\mathcal{A}}(h_n|I_n)$ be the *posteriori* probabilities of labeling h_n at voxel n for the reference manual and the automated segmentation, respectively. Then the L_1 tissue classification error between the two segmentations is defined as

$$L_1 = \frac{1}{2N}\sum_{n=1}^{N}\sum_{i=1}^{m}|p^{\mathcal{A}}(h_i|I_n) - p^{\mathcal{R}}(h_i|I_n)|. \quad (13)$$

In the case of perfectly overlapping labeling of voxels, $L_1 = 0$. In reality, L_1 is a measure of the cost of mislabeling the voxels with respect to the reference manual segmentation.

We compute the L_1 errors for each algorithm, i.e., LDDMM and greedy algorithm with respect to the same set of manual segmentations. Automated segmentations via the greedy algorithm have been obtained previously [3], [23] using established protocols. Briefly, these mapping protocols involve a first step of coarse alignment of the region of interest (containing the hippocampus) based on manually delineated landmarks between the template and the target scans [31], and a second step of ap-plying the greedy algorithm to the MR subvolume of the region of interest. The template hippocampal segmentation is carried forward through the concatenation of the two steps into the target scan, resulting in automated segmentation of the hippocampus. To compare LDDMM and the greedy algorithm, we replace the greedy algorithm in the second step with LDDMM. Table I shows that the two algorithms produce automated segmentations that are comparable.

B. Validation 2: Initial Velocity Vector Fields vs Linear Displacement Vector Fields

We have already demonstrated that differences due to DAT in brain structures such as the hippocampus could be observed by analyzing the displacement vector fields between the DAT and control subjects [3], [4]. Since the initial velocity v_0 field from the template parameterizes the entire geodesic [13], [32], we should expect the final displacement u to be highly correlated with the initial velocity v_0. Since the initial velocity vector fields v_0 are computed on the 3-D volumetric submanifold $\mathcal{M}_0$, and the displacement vector fields from [4] are computed on the 2-D surface submanifold (the triangulated surface around the boundary of $\mathcal{M}_0$), we interpolate v_0 onto the surface for computing the correlation. The displacement vector fields u are computed also on the surface, by taking the difference between each target point and its corresponding starting point.

At each surface point, we compute the Spearman rank-order correlation between the surface-interpolated v_0 and surface displacement u in x, y, and z directions. Since possible outlying points well away from the main body of the data could unduly influence the calculation of the correlation coefficient, a nonparametric procedure, due to Spearman, is to replace the observations by their ranks in the calculation of the correlation coefficient. The Rank Correlation test is a distribution free test that determines whether there is a monotonic relation between two variables. A monotonic relation exists when any increase in one variable is invariably associated with either an increase or a decrease in the other variable. Significance of correlation is adjusted to be $\alpha = 0.05/(3 \times 12167) = 1.3698 \times 10^{-6}$ (the left and right surfaces have a total of 12167 points). Table II summarizes the correlations in the x, y and z directions. The correlations are visualized on the template surface in Fig. 2, where the significant correlations are painted as a flame scale onto each surface point. Surface points for which correlations are not significant are painted yellow-green.

C. PCA and Statistics on Lv_0

Permutation tests are performed on the left- and right-hand sides separately. For the left hippocampus, the first 20 principal components accounting for 82.9% of the total variance are used. For the right hippocampus, the first 20 principal components accounting for 80.5% of the total variance are used.

In Fig. 3 (3a) and (3b), we plot the empirical distribution $\widehat{F}$ from randomized Hötelling's T^2 test with 10 000 group permutations, between the CDR 0 and CDR 0.5 subjects. The p values shown are calculated from (12). There is a group difference ($p = 0.0074$) on the left-hand side but no group difference on the statistic that right-hand side ($p = 0.07$).

The principal component values of the left hippocampus are then used in a "leave-one-out" logistic regression classification procedure that selects subsets of principal components that discriminate the two subject groups [33]. Logistic regression analysis is often used to investigate the relationship between discrete responses (e.g., success or failure; normal, mild or severe) and a set of explanatory variables [34], [35]. It fits linear logistic regression models for discrete response data by the method of maximum likelihood. In the stepwise procedure, at each step the candidate explanatory variable with the largest χ^2 statistic that satisfies a predetermined selection criterion (e.g., $p = 0.05$) will be selected into the model. At each step among the selected variables, the one with the smallest χ^2 statistic that satisfies a pre-determined exclusion criterion (e.g., $p = 0.2$) will be removed from the model. The logistic regression procedure terminates when no more variables satisfy the inclusion or removal criteria. Using the solution of left-side principal components 2, 11, 14, (likelihood ratio: $\chi^2 = 19.6$, $df = 3$, $p = 0.0002$) to discriminate the two groups with correct classification rate of 84.6% (22 out of 26) for the CDR 0 group and 66.7% (12 out of 18) for the CDR 0.5 group.

To assess the stability of the discriminating solution sets, we randomly divided each clinical group into 9 subgroups of 2 to 3 subjects each. This creates 9 trials. In each trial, we use the 90% majority of the subjects from each clinical group in a stepwise "leave-one-out" logistic regression procedure that selects a subset of the principal components. We then classify the smaller set of subjects according to the subset solution. Across 9 trials, the principal component (PC) 2 is selected each time; PC 11 six times; PC 14 six times; and PC 12 three times. The overall rate of correct classification across the nine trials is 81.1% (92.6% for CDR 0 and 66.7% for CDR 0.5 subjects).

IV. Discussion

The purpose of computing the initial velocity vector fields is to enable us to analyze the geodesic resulting from the large-deformation transformation which is not possible from analyzing displacement vector fields under small-deformation assumption. In [13] the authors showed that PCA models based on point data [36] are not always able to generate acceptable shapes in the space of given shapes. For example, these models do not account for the curved manifold of shape space, unlike analysis based on diffeomorphism (i.e., PCA on initial momentum).

It is interesting to note that there are a number of surface points in the hippocampus for which v_0 and u are not significantly correlated. This could be a reflection of the fact u is calculated using linearizing assumptions whereas v_0 is calculated in the large deformation setting without the linearizing assumptions, such that if the points follow "curved" trajectories, then the u displacement field will not correlate with the initial velocity field, v_0.

In this paper, PCA analysis shows a left hippocampal shape abnormality in the CDR 0.5 group as compared to the CDR 0 group. This is consistent with our previous follow-up study of a group of CDR 0 subjects who later progress to CDR 0.5 [6]. Discriminant analysis shows a somewhat improved overall classification rates compared with our previous cross-sectional study (in [3], 78% for CDR 0, 67% for CDR 0.5), based on the greedy algorithm implementation of the diffeomorphic mapping and comparing displacement vector fields: there were 31 overlapping subjects between the two studies, and of these 31 subjects, six were correctly classified in the current study whereas in the previous study they were misclassified, and two were misclassified in the current study whereas in the previous study they were corrected classified. Even though McNemar's test [37] did not show disagreement between the two studies ($S = 2.0$, $df = 1$, $p = 0.16$), this was probably due to the small number of shared subjects. If the number of subjects were to double while keeping the same correct classification rates, McNemar's test would have shown an improvement of the current study over the previous study ($S = 4.0$, $df = 1$, $p = 0.045$)! Further, validation using new subjects that are unrelated to training (or model building) data is needed in the future to test the validity of this approach.

The results of the current study by no means dispute findings of recent studies that show longitudinal changes in structure to be a more sensitive marker than cross-sectional comparisons in AD [38]-[45]. Rather, based on the findings of this study that within the cross-sectional setting, statistics on the initial momentum fields is more powerful than on the linear displacements, we believe that analysis of longitudinal changes of brain structures based on initial momentum will further improve the sensitivity and specificity of AD detection. In addition, analysis of initial momentum based on the subfields of the hippocampus may give better understanding of the regional abnormalities associated with DAT, as has been demonstrated by a similar analysis of linear displacements [7].

Acknowledgments

This work was supported in part by the National Institutes of Health (NIH) under Grant P50-MH71616, Grant R01-MH60883, Grant R01-MH56584, Grant R01-MH064838, Grant P01-AG03991, Grant R01-AG025824, and P50-AG05681, AG05684, in part by the National Center for Research Resources under Grant P41-RR15241, in part by the National Science Foundation under Grant DMS-0456253, in part by the Natural Sciences and Engineering Research Council (Canada) under Grant 31-611387, and in part by a grant from the HIGHQ Foundation (Canada).

REFERENCES

[1]. Grenander U, Miller MI. Computational anatomy: An emerging discipline. Quart. Appl. Math. Dec..1998 vol. LVI:617–694.

[2]. Csernansky JG, Wang L, Joshi SC, Ratnanather JT, Miller MI. Computational anatomy and neuropsychiatric disease: Probabilistic assessment of variation and statistical inference of group difference, hemispheric asymmetry, and time-dependent change. NeuroImage. 2004; vol. 23:S56–S68. [PubMed: 15501101]

[3]. Csernansky JG, Wang L, Joshi S, Miller JP, Gado M, Kido D, McKeel D, Morris JC, Miller MI. Early dat is distinguished from aging by high-dimensional mapping of the hippocampus. Neurology. 2000; vol. 55(no. 11):1636–1643. [PubMed: 11113216]

[4]. Wang L, Swank JS, Glick IE, Gado MH, Miller MI, Morris JC, Csernansky JG. Changes in hippocampal volume and shape across time distinguish dementia of the alzheimer type from healthy aging. NeuroImage. 2003; vol. 20(no. 2):667–682. [PubMed: 14568443]

[5]. Csernansky JG, Hamstra J, Wang L, McKeel D, Price JL, Gado M, Morris JC. Correlations between antemortem hippocampal volume and postmortem neuropathology in AD subjects. Alzheimer Dis. Assoc. Disord. 2004; vol. 18(no. 4):190–195. [PubMed: 15592129]

[6]. Csernansky JG, Wang L, Swank J, Miller JP, Gado M, McKeel D, Miller MI, Morris JC. Preclinical detection of alzheimer's disease: Hippocampal shape and volume predict dementia onset in the elderly. NeuroImage. 2005; vol. 25(no. 3):783–792. [PubMed: 15808979]

[7]. Wang L, Miller JP, Gado MH, McKeel DW, Rothermich M, Miller MI, Morris JC, Csernansky JG. Abnormalities of hippocampal surface structure in very mild dementia of the alzheimer type. NeuroImage. 2006; vol. 30(no. 1):52–60. [PubMed: 16243546]

[8]. Holm DD, Ratnanather JT, Trouvé A, Younes L. Soliton dynamics in computational anatomy. NeuroImage. 2004; vol. 23:S170–S178. [PubMed: 15501086]

[9]. Beg MF, Miller MI, Trouvé A, Younes L. Computing large deformation metric mappings via geodesic flows of diffeomorphisms. Int. J. Comput. Vis. 2005; vol. 61(no. 2):139–139.

[10]. Miller MI, Trouvé A, Younes L. Geodesic shooting for computational anatomy. J. Math. Imag. Vis. 2006; vol. 24(no. 2):209–228.

[11]. Arnold, VI. Mathematical Methods of Classical Mechanics. 2nd ed. Springer; New York: 1989.

[12]. Helm P, Younes L, Beg MF, Ennis D, Leclercq C, Faris O, McVeigh E, Miller M, Winslow R. Evidence of structural remodeling in the dyssynchronous failing heart. Circ. Res. 2006; vol. 98(no. 1):125–132. [PubMed: 16339482]

[13]. Vaillant M, Miller MI, Younes L, Trouvé A. Statistics on diffeomorphisms via tangent space representations. NeuroImage. 2004; vol. 23:S161–S169. [PubMed: 15501085]

[14]. Dupuis P, Grenander U, Miller M. Variational problems on flows of diffeomorphisms for image matching. Quart. Appl. Math. Sep..1998 vol. LVI:587–600.

[15]. Trouvé A. An infinite dimensional group approach for physics based models in patterns recognition. Int. J. Comput. Vis. 1995; vol. 28(3):213–221.

[16]. Christensen GE, Rabbitt RD, Miller MI. 3D brain mapping using a deformable neuroanatomy. Phys. Med. Biol. Mar..1994 vol. 39:609–618. [PubMed: 15551602]

[17]. Trouvé A. Diffeomorphism groups and pattern matching in image analysis. Int. J. Comput. Vis. 1998; vol. 28(no. 3):213–221.

[18]. Miller MI. Computational anatomy: Shape, growth, and atrophy comparison via diffeomorphisms. NeuroImage. 2004; vol. 23:S19–S33. [PubMed: 15501089]

[19]. Joshi, S.; Banerjee, A.; Christensan, GE.; Csernansky, JG.; Haller, JW.; Miller, MI.; Wang, L. Gaussian random fields on sub-manifolds for characterizing brain surfaces. In: Duncan, JS.; Gindi, G., editors. The 15th International Conference on Information Processing in Medical Imaging, IPMI'97; 1997; Berlin, Germany: Springer-Verlag; p. 381-386.ser. Lecture Notes in Computer Science

[20]. Joshi, SC. Ph.D. dissertation. Dept. Elect. Eng., Sever Inst. Technol., Washington Univ.; St. Louis, MO: 1997. Large deformation diffeomorphisms and gaussian random fields for statistical characterization of brain submanifolds.

[21]. Van Trees, HL. Detection, Estimation and Modulation Theory, Part I. Wiley; New York: 1968.

[22]. Anderson, TW. An Introduction to Multivariate Statistical Analysis. Wiley; New York: 1958.

[23]. Haller JW, Banerjee A, Christensen GE, Gado M, Joshi SC, Miller MI, Sheline Y, Vannier MW, Csernansky JG. 3D hippocampal morphometry by high dimensional transformation of a neuroanatomical atlas. Radiology. Feb..1997 vol. 202:504–510. [PubMed: 9015081]

[24]. Wang L, Joshi SC, Miller MI, Csernansky JG. Statistical analysis of hippocampal asymmetry in schizophrenia. NeuroImage. Sep..2001 vol. 14:531–545. [PubMed: 11506528]

[25]. Morris JC. The clinical dementia rating (CDR): Current version and scoring rules. Neurology. 1993; vol. 43(no. 11):2412–2414. [PubMed: 8232972]

[26]. Berg L, McKeel DW Jr. Miller JP, Storandt M, Rubin EH, Morris JC, Baty J, Coats M, Norton J, Goate AM, Price JL, Gearing M, Mirra SS, Saunders AM. Clinicopathologic studies in cognitively healthy aging and alzheimer's disease: Relation of histologic markers to dementia severity, age, sex, and apolipoprotein e genotype. Arch. Neurol. 1998; vol. 55(no. 3):326–335. [PubMed: 9520006]

[27]. Petersen RC, Doody R, Kurz A, Mohs RC, Morris JC, Rabins PV, Ritchie K, Rossor M, Thal L, Winblad B. Current concepts in mild cognitive impairment. Arch. Neurol. 2001; vol. 58(no. 12): 1985–1992. [PubMed: 11735772]

[28]. Grant EA, Miller JP, Morris JC. Longitudinal course and neuropathologic outcomes in original vs revised MCI and in pre-MCI. Neurology. Aug..2006 vol. 67:467–473. [PubMed: 16894109]

[29]. Joshi M, Cui J, Doolittle K, Joshi S, Essen DV, Wang L, Miller MI. Brain segmentation and the generation of cortical surfaces. NeuroImage. 1999; vol. 9(no. 5):461–476. [PubMed: 10329286]

[30]. Ratnanather JT, Wang L, Nebel MB, Hosakere M, Han X, Csernansky JG, Miller MI. Validation of semiautomated methods for quantifying cingulate cortical metrics in schizophrenia. Psychiatry Res. 2004; vol. 132(no. 1):53–68. [PubMed: 15546703]

[31]. Joshi, S.; Miller, M.; Christensen, G.; Banerjee, A.; Coogan, T.; Grenander, U. Hierarchical brain mapping via a generalized dirichlet solution for mapping brain manifolds. Proc. SPIE Int. Symp. Optical Science, Engineering, and Instrumentation (Vision Geometry IV); San Diego, CA. 1995; p. 278-289.

[32]. Miller MI, Banerjee A, Christensen GE, Joshi SC, Khaneja N, Grenander U, Matejic L. Statistical methods in computational anatomy. Statist. Meth. Med. Res. 1997; vol. 6(no. 3):267–299.

[33]. SAS System for Windows, V8. SAS Institute, Inc.; Cary, NC: 2000.

[34]. Hosmer, DW., Jr.; Lemeshow, S. Applied Logistic Regression. second ed. Wiley; New York: 2000.

[35]. Stokes, M.; Davis, C.; Koch, G. Categorical Data Analysis Using the SAS System. 2nd ed. SAS Institute, Inc.; Cary, NC: 2000.

[36]. Cootes T, Taylor C, Cooper D, Graham J. Active shape models—Their training and application. Comput. Vis. Image Understanding. 1995; vol. 61:38–59.

[37]. McNemar Q. Note on the sampling error of the difference between correlated proportions or percentages. Psychometrika. 1947; vol. 12:153–157. [PubMed: 20254758]

[38]. Du A-T, Schuff N, Chao LL, Kornak J, Jagust WJ, Kramer JH, Reed BR, Miller BL, Norman D, Chui HC, Weiner MW. Age effects on atrophy rates of entorhinal cortex and hippocampus. Neurobiol. Aging. May.2006 vol. 27:733–740. [PubMed: 15961190]

[39]. Jack CR, Shiung MM, Weigand SD, O'Brien PC, Gunter JL, Boeve BF, Knopman DS, Smith GE, Ivnik RJ, Tangalos EG, Petersen RC. Brain atrophy rates predict subsequent clinical conversion in normal elderly and amnestic MCI. Neurology. Oct..2005 vol. 65:1227–1231. [PubMed: 16247049]

[40]. Mungas D, Harvey D, Reed BR, Jagust WJ, DeCarli C, Beckett L, Mack WJ, Kramer JH, Weiner MW, Schuff N, Chui HC. Longitudinal volumetric MRI change and rate of cognitive decline. Neurology. Aug..2005 vol. 65:565–571. [PubMed: 16116117]

[41]. Leow AD, Klunder AD, Jack CR, Toga AW, Dale AM, Bernstein MA, Britson PJ, Gunter JL, Ward CP, Whitwell JL, Borowski BJ, Fleisher AS, Fox NC, Harvey D, Kornak J, Schuff N, Studholme C, Alexander GE, Weiner MW, Thompson PM. For the ADNI preparatory phase study, longitudinal stability of MRI for mapping brain change using tensor-based morphometry. NeuroImage. Feb..2006

[42]. Barnes J, Godbolt AK, Frost C, Boyes RG, Jones BF, Scahill RI, Rossor MN, Fox NC. Atrophy rates of the cingulate gyrus and hippocampus in AD and FTLD. Neurobiol. Aging. Jan..2006

[43]. Frost C, Kenward MG, Fox NC. The analysis of repeated 'direct' measures of change illustrated with an application in longitudinal imaging. Statist. Med. Nov..2004 vol. 23:3275–3286.

[44]. Barnes J, Scahill RI, Boyes RG, Frost C, Lewis EB, Rossor CL, Rossor MN, Fox NC. Differentiating AD from aging using semiautomated measurement of hippocampal atrophy rates. NeuroImage. Oct..2004 vol. 23:574–581. [PubMed: 15488407]

[45]. Scahill RI, Frost C, Jenkins R, Whitwell JL, Rossor MN, Fox NC. A longitudinal study of brain volume changes in normal aging using serial registered magnetic resonance imaging. Arch. Neurol. Jul..2003 vol. 60:989–994. [PubMed: 12873856]

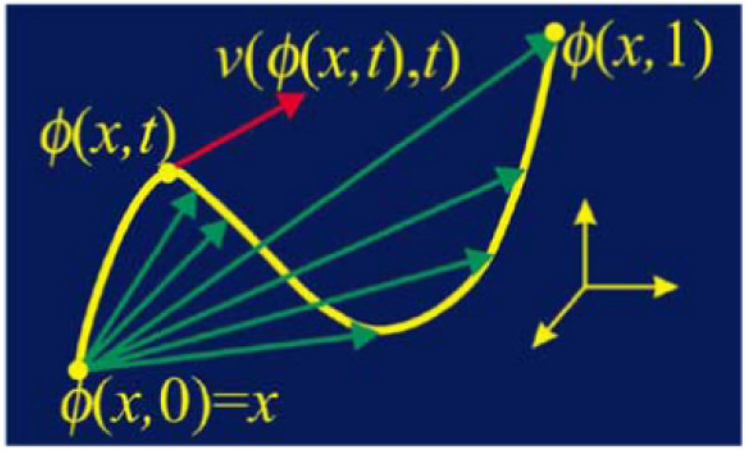

Fig. 1.
Diffeomorphic flow.

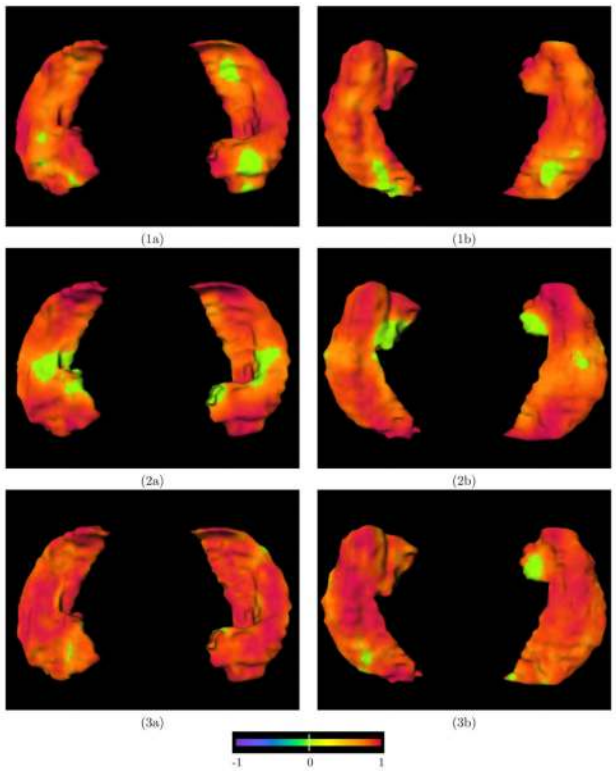

Fig. 2.

Correlations between displacement vector fields (u) and initial velocity vector fields (v_0). Only the surface vertices that show significant correlation were colored according to the correlation, others were colored as yellow-green. Top, middle and bottom row shows correlation between v_0 and u along the x, y, and z axes, respectively. Column a shows dorsal view (from the top) and column b shows ventral view (from the bottom) of the hippocampus.

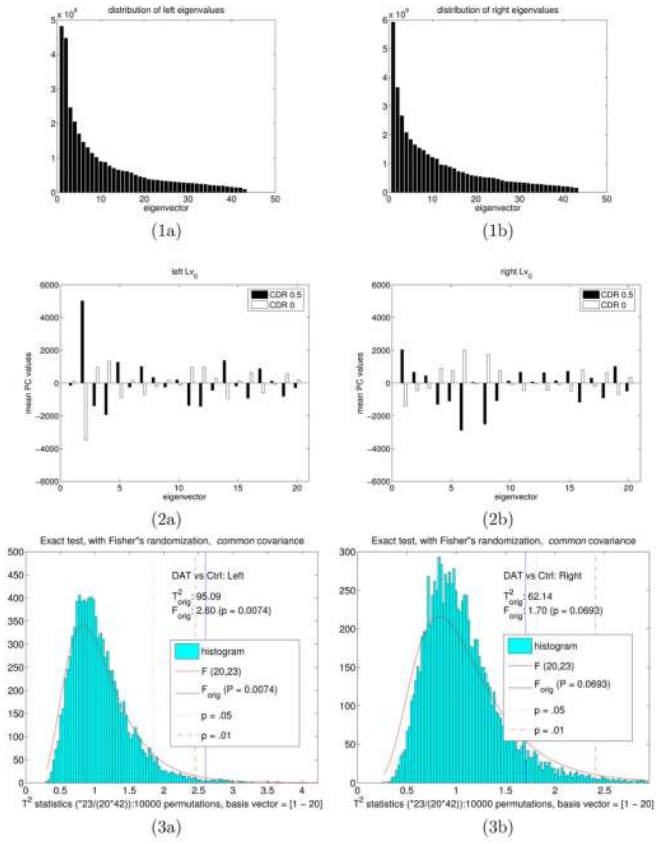

Fig. 3.

PCA of Lv_0. Row (1) shows the distribution of eigenvalues for all eigenfunctions. Row (2) shows the distribution of mean coefficients (CDR 0 and CDR 0.5 groups) associated with the first 20 principal components. Row (3) shows the permutation tests for group differences using the first 20 principal components. The p values shown are calculated from [see (12)].

Also shown are: 1) $\widehat{F}\left(T^2\right)$ value (solid blue line) of the Control-versus-DAT group comparison; 2) theoretical F-distribution (solid red curve) with (20,23) degrees of freedom superimposed on the empirical distribution; 3) $p = .05$ (red dotted line) and $p = .01$ (red dot-dash line) for reference. Column (a) is for the left hippocampus where the first 20 principal components account for 82.9% of the total variance. Column (b) is for the right hippocampus where the first 20 principal components account for 80.5% of the total variance.

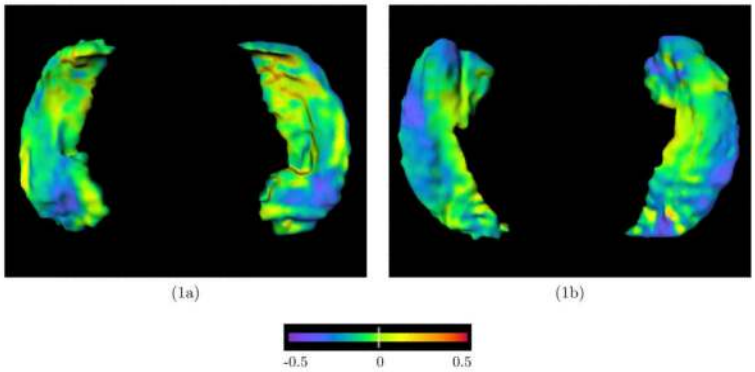

Fig. 4.

Visualization of the pattern of hippocampal deformities in subjects with very mild DAT (CDR 0.5) compared with nondemented subjects (CDR 0) (Data taken from [3]). The flame coloring represents the z-scores between the two groups of subjects. Inward variation of the hippocampal surface is represented by cooler colors (i.e., blue to purple), while outward variation is represented by warmer colors (i.e., orange to red). In (1a) the pair of hippocampal surfaces are shown from above, with the head of the hippocampus pointing toward the bottom edge of the figure panel, and the left hippocampus is on the right-hand side of the panel. In (1b) the hippocampal surfaces are shown from below, with the head of the hippocampus pointing toward the top edge of the figure panel, and the left hippocampus is on the right-hand side of the panel.

Table I

Validation 1—Matching Errors Between Each Algorithm and the Same Set of Manual Segmentations. Study 1: Five Schizophrenia and Five Control Subjects (MR Data Taken From [23]). Study 2: Five Dementia of the Alzheimer Type (DAT) and Five Control Subjects (MR Data Taken From [3])

Study	Algorithm	L_1 Error	% Voxel Overlap
Study 1	Greedy	0.230 (±0.025)	79.45 (±2.97)
	LDDMM	0.226 (±0.026)	79.56 (±2.72)
Study 2	Greedy	0.220 (±0.048)	80.62 (±5.52)
	LDDMM	0.201 (±0.026)	78.54 (±5.80)

Table II

Validation 2—Correlations Between Initial Velocity Vector Fields (v_0) and Displacement Vector Fields (u). After Adjusting for Multiple Comparisons, the Number of Surface Vertices That Show Significant Correlation is Shown as a Percentage of Total Number of Surface Vertices

Axis	Mean	Median	Range	% Surface Vertices
x	0.82 (±0.08)	0.89	0.64 – 1.00	95.4
y	0.87 (±0.09)	0.88	0.64 – 0.99	90.4
z	0.88 (±0.07)	0.89	0.64 – 0.99	97.8